Clim Dyn
DOI 10.1007/s00382-017-3848-x

Predictability of summer extreme precipitation days over eastern China

Juan Li[1,2] · **Bin Wang**[1,2]

Received: 24 April 2017 / Accepted: 29 July 2017

Abstract Extreme precipitation events have severe impacts on human activity and natural environment, but prediction of extreme precipitation events remains a considerable challenge. The present study aims to explore the sources of predictability and to estimate the predictability of the summer extreme precipitation days (EPDs) over eastern China. Based on the region- and season-dependent variability of EPDs, all stations over eastern China are divided into two domains: South China (SC) and northern China (NC). Two domain-averaged EPDs indices during their local high EPDs seasons (May–June for SC and July–August for NC) are therefore defined. The simultaneous lower boundary anomalies associated with each EPDs index are examined, and we find: (a) the increased EPDs over SC are related to a rapid decaying El Nino and controlled by Philippine Sea anticyclone anomalies in May–June; (b) the increased EPDs over NC are accompanied by a developing La Nina and anomalous zonal sea level pressure contrast between the western North Pacific subtropical high and East Asian low in July–August. Tracking back the origins of these boundary anomalies, one or two physically meaningful predictors are detected for each regional EPDs index. The causative relationships between the predictors and the corresponding EPDs over each region are discussed using lead-lag correlation analyses. Using these selected predictors, a set of Physics-based Empirical models is derived. The 13-year (2001–2013) independent forecast shows significant temporal correlation skills of 0.60 and 0.74 for the EPDs index of SC and NC, respectively, providing an estimation of the predictability for summer EPDs over eastern China.

Keywords Extreme precipitation · Eastern China · Physics-based empirical model · Seasonal predictability · Seasonal prediction · East Asian summer monsoon

1 Introduction

Extreme precipitation events have severe impacts on society, economy and environment (Easterling et al. 2000; Meehl et al. 2000; Lesk et al. 2016), while climate change has the potential to increase the frequency and intensity of extreme precipitation (Meehl et al. 2007; Donat et al. 2016). As one of the most populous countries in the world, China is vulnerable to natural catastrophes such as flood triggered by extreme precipitation. In the twentieth century, 18 of the world's 100 most expensive natural disasters occurred in China, and 12 of them were due to extreme flood (http://www.disastercenter.com/disaster/TOP100C.html). Influenced by the Asian monsoon system, eastern China has large precipitation variability, leading to higher frequency of flood or drought. During 21–22 July of 2012, Beijing experienced severe extreme rainfall, which influenced 1.9 million people

This paper is a contribution to the special issue on East Asian Climate under Global Warming: Understanding and Projection, consisting of papers from the East Asian Climate (EAC) community and the 13th EAC International Workshop in Beijing, China on 24-25 March 2016, and coordinated by Jianping Li, Huang-Hsiung Hsu, Wei-Chyung Wang, Kyung-Ja Ha, Tim Li, and Akio Kitoh.

✉ Bin Wang
wangbin@hawaii.edu

Juan Li
juanl@hawaii.edu

[1] Earth System Modeling Center, Nanjing University of Information Science and Technology, Nanjing, China

[2] Department of Atmospheric Sciences, International Pacific Research Center, SOEST, University of Hawaii at Manoa, Honolulu, HI, USA

Published online: 20 August 2017

and caused more than $1.6 billion economic loss (Zhou et al. 2013). Skillful prediction of extreme precipitation events would be immensely beneficial to disaster mitigation and adaptation planning. Thus, accurate prediction of extreme precipitation over eastern China has become an increasing societal and scientific demand nationwide.

Previous studies have discussed the changes in extreme precipitation events over China in the recent decade (Zhang et al. 2008; Choi et al. 2009; Tu et al. 2010; You et al. 2010; Li et al. 2012, 2017a; Wang and Yang 2017). It was found that the extreme precipitation exhibited a significant increasing trend over the Yangtze River, southwest and south China during 1951–2000 (Zhai et al. 2005). Significant increases in heavy precipitation were found at both rural and urban stations in eastern China during 1955–2011 (Liu et al. 2015). The physical causes linked to extreme precipitation over China were also explored. Weng et al. (2004) showed that the western Pacific subtropical high and the mid-latitude wave systems had great effects on the summer extreme wet events over China. Orsolini et al. (2015) revealed that the Silk-Road and polar wave trains played a key role in modulating extreme precipitation over north and northeast China. Simulations from a regional climate model indicated that the increasing number of heavy rain days over some parts of China was attributable to greenhouse effect (Gao et al. 2002). Global warming rather than aerosol effects was suggested as a cause of the changes in heavy rainfall in eastern China (Liu et al. 2015).

Although physical causes of extreme precipitation have been explored, its prediction is rarely documented. While prediction of seasonal mean rainfall in dynamical models has little skill over subtropical land (Wang et al. 2009a), it is perhaps more difficult to forecast the extreme precipitation due to its infrequent and irregular occurrence. Therefore, prediction of extreme precipitation over eastern China remains a big challenge. To what extent are the summer extreme precipitation days (EPDs) over eastern China predictable? To answer this question, understanding the origins of the predictability of summer EPDs is the first step. Taking physical mechanisms into account, the physics-based empirical (P–E) model can be built to estimate the predictability. The P–E model approach might be effective since it has been successfully applied to seasonal predictability studies of a variety of meteorological phenomena (Yim et al. 2014; Wang et al. 2015a, b; Grunseich and Wang 2016; Li and Wang 2016; Xing et al. 2016; Li et al. 2017b; Zhu and Li 2017).

Aiming to explore the predictability of EPDs over eastern China, this paper is organized as follows. Section 2 introduces data and methodology. In Sect. 3, definition of EPDs and regional EPDs indices are presented. Simultaneous lower boundary anomalies associated with the regional EPDs indices over eastern China are explored in Sect. 4. Section 5 investigates the lead-lag relationship between physical predictors and predictands. Predictability of summer EPDs over eastern China is assessed in Sect. 6. Major findings are summarized in Sect. 7.

2 Data and methods

2.1 Data

Daily precipitation records of 746 stations over China for the period of 1979–2013 were utilized. This dataset was obtained from the National Meteorological Information Center of China Meteorological Administration. A homogenized daily mean temperature dataset (Li et al. 2016) derived from 753 stations in China during 1979–2013 was also employed. Stations with more than 10% records missing in any given year were excluded.

Monthly mean sea surface temperature (SST) data were derived from an arithmetic mean of two datasets: the Hadley Centre Sea Ice and Sea Surface Temperature (HadISST) (Rayner et al. 2003) and the National Oceanic and Atmospheric Administration Extended Reconstructed SST (ERSST) version 4 (Huang et al. 2015). The monthly sea level pressure (SLP), 2-meter temperature, 200 hPa geopotential height and 850 hPa winds were obtained from the ERA-Interim Reanalysis (Dee et al. 2011). The global monthly mean precipitation data from Global Precipitation Climatology Project (GPCP, v2.3) datasets (Adler et al. 2003) were employed to analyze the global precipitation. All the datasets cover the period of 1979–2013.

2.2 Methodology for physics-based empirical model and validation

Different from traditional statistical models, only physically meaningful predictors are selected, which is the primary principle of establishing P–E model (Wang et al. 2015b). Emphasis is placed on the physical interpretation of selected predictors. Statistically, the first step is to use lead-lag correlation maps between the predictand and only lower boundary anomalies (such as SST, 2-m temperature and SLP) before the target month to detect only two types of predictive signals: (a) the persistent signals that often signify the slow variation of the lower boundary anomalies which will "persist" into the next season, and (b) the tendency signals that reflect the direction of subsequent evolution. Here, the persistent signals are derived from two months mean before the target season, such as March–April mean when forecast season is May–June. Tendency signals are obtained from winter (Dec.–Jan.) to the two months before target season, such as Dec.–Jan. to May–June when forecast season is July–August.

Because we focus on large-scale signals, in the second step, the predictors are defined in a large area but the lead-lag correlation is taken into account only over those grid points where the correlation coefficient is significant at the 0.95 confidence level (Lee et al. 2013). Thus, here the predictors are defined by:

$$\mathrm{Pred(t)} = [\mathrm{TF(t, lat, lon)} \times \mathrm{TCC(lat, lon)}], \text{ if } |\mathrm{TCC(lat, lon)}| > 0.42 \text{ (95\% confidence level)},$$

where TF denotes the value of a predictor (SST, 2-m temperature or SLP) at lead time *t* and at each grid, TCC is the temporal correlation coefficient between the predictand and TF values at each gird during 1979–2000, and square brackets denote the areal mean over the selected regions. For instance, the March–April mean SLP with absolute value of TCC larger than 0.42 (95% confidence level), weighted by TCC and averaged over the selected region (the box in Fig. 7a), is defined as predictor SC-a.

After above-mentioned two steps, several physical meaningful predictors are considered as candidates. Then, stepwise regression is used to build the P–E model. The fundamental rule of the stepwise regression procedure is to select most significant variables and remove the one significant related to the most significant variables. In other words, if two selected variables are highly correlated with each other, the procedure will remove the less significant one. Therefore, stepwise regression can identify important predictors and ascertain the mutual independency of predictors. A 99% confidence level for Fisher's *F* test is used as the criterion to select predictors.

To verify the prediction skill, two validation methods (Wang et al. 2015b; Li and Wang 2016) are applied. (1) *Leave-three-out cross-validated reforecast* (Geisser 1975; Blockeel and Struyf 2003). To alleviate the over-fitting problem, 3 years centered on a target year are withheld from the training sample, and the regression model is built to forecast the target year. Then, the process is repeated for all the other years to get the cross-validated reforecast for 1979–2000. (2) *Independent forecast*. The stepwise regression model is built with the training data for 1979–2000, and independent forecast is then made for the rest 13-year during 2001–2013. All predictors are selected from the period of 1979–2000 to avoid the artificial bias caused by the period overlapping in predictor selection and verification.

In addition to TCC, the Mean Square Skill Score (MSSS) is used to measure the deterministic seasonal forecast skill (Murphy 1988; WMO 2002). The MSSS indicates the percentage reduction in mean square error of the model forecast compared to the climatology "forecast". Positive (negative) skill means that the model forecast is better (worse) than the climatology "forecast".

3 Definition of EPDs and regional EPDs indices

Considering regional differences, percentile-based extreme precipitation index is defined, which is similar to previous studies (Alexander et al. 2006; Moberg et al. 2006). For a given station, an extreme precipitation event is defined if the daily precipitation is beyond the 90th percentile threshold of all rainy records (daily rainfall >0.1 mm) for the whole 35 years (1979–2013). Each station defines its own threshold in the same manner.

Figure 1a displays the 90th percentile threshold of daily precipitation across China. The thresholds gradually increase from northwest to southeast of China, ranging from 4 to 40 mm. It is similar to the spatial distribution of May–August (MJJA) mean precipitation (figure not shown) since the 90th percentile threshold of daily precipitation is mainly determined by summer precipitation. The number of days when the daily precipitation exceeds the corresponding threshold is regarded as EPDs. Note that the variability of EPDs defined here is robust and not sensitive to the chosen thresholds.

How much is the difference between the mean value and the 90th percentile of daily precipitation? The annual mean precipitation shows a larger amount in southern China and gradually decreases toward northern China (Fig. 1b). The ratio of 90th percentile threshold to annual mean precipitation is presented in Fig. 1c. The ratio is higher in northern China, especially in northwestern China, while the ratio is lower in southern China. This is due to the fact that in dry regions, the variability of daily precipitation is much larger than that in wet regions. Note that, over the lower reaches of Yellow River, the annual mean precipitation has little difference between the east and west, but the threshold value is higher in the east than in the west, indicating that the variability of daily precipitation is stronger in the east than in the west.

Since the occurrence of strong precipitation events is mainly confined to eastern China, the present study only focuses on the EPDs over eastern China. May through August is the primary rainy season over East Asia (Wang and LinHo 2002; Wang et al. 2009b). What is the extreme rainfall season over eastern China? Figure 2a shows the seasonal march of climatological monthly mean EPDs from April to September. Evidently, large values of climatological EPDs mainly appear from May to August, and from south to north progressively. Similar northward progression can be found in the seasonal evolution of heavy rainfall (daily rainfall >50 mm) days, but the heavy rainfall is mainly seen in the south of Yellow River (Fig. 2b). Thus, the months of MJJA can be considered as the extreme rainfall season over eastern China. Note that the maximum center of EPDs mainly occurs in South China (SC, south of 30°N) during May–June (MJ), while large value of EPDs concentrates in

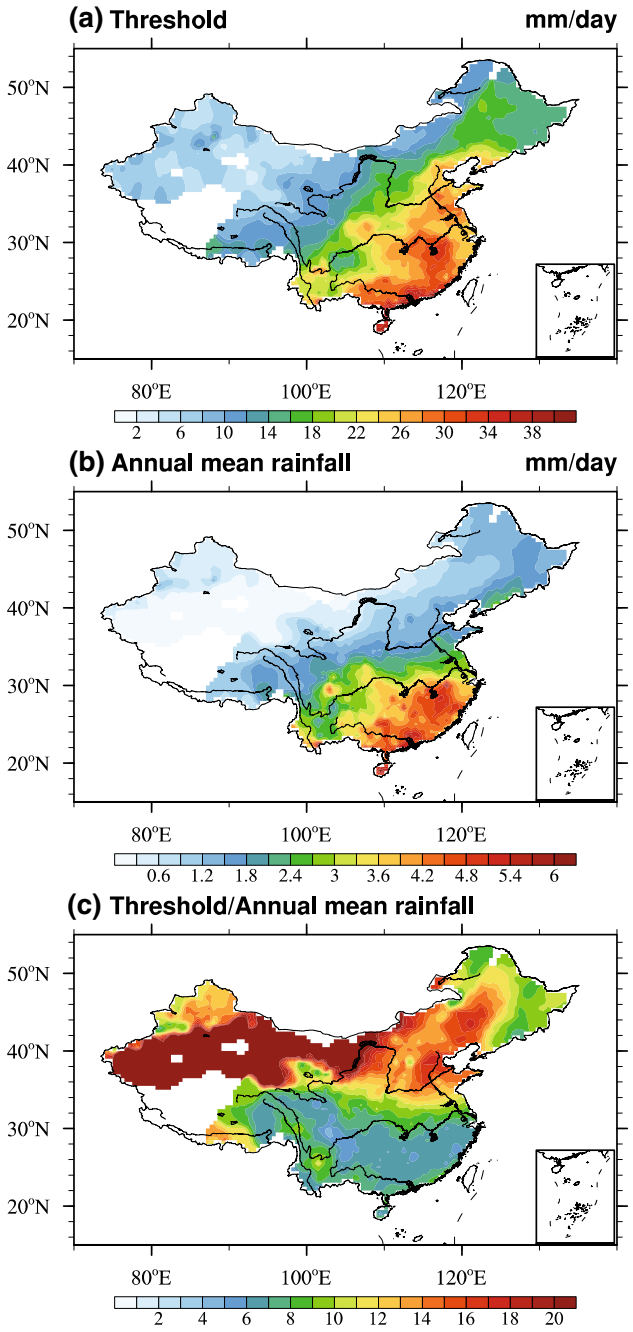

Fig. 1 **a** Threshold values (mm/day) defined for extreme precipitation over China. At each station, the 90th percentile of daily precipitation within all rainy days during 1979–2013 is defined as the threshold. **b** The climatological annual mean precipitation (mm/day) during 1979–2013. **c** The ratio of threshold to climatological annual mean precipitation

northern China (NC, north of 30°N) during July–August (JA). Based on this feature of the seasonal march of EPDs, all stations over eastern China are divided into two domains: SC and NC.

Figure 3 shows the climatological annual cycle of EPDs (red bar) averaged over SC and NC. The EPDs averaged over SC have a peak in MJ, while EPDs over NC have a peak in JA. The corresponding annual variations of the monthly mean precipitation (blue bar in Fig. 3) show the same feature. Therefore, MJ and JA could be considered as the local summer rainfall season for SC and NC, respectively. Then two areal-mean EPDs indices, namely EPDs-SC and EPDs-NC, are defined at each domain during their local summer rainfall season, so as to facilitate the understanding and prediction of the variability of EPDs over eastern China.

The time series of EPDs-SC and EPDs-NC are displayed in Fig. 4. It is noted that the EPDs-SC (EPDs-NC) and the corresponding seasonal mean precipitation averaged over SC (NC) exhibit extremely coherent year-to-year variation. Their TCC for SC (NC) is 0.98 (0.96), indicating that the seasonal EPDs and seasonal mean rainfall over eastern China may share very similar sources of predictability. Interestingly, corresponding to a weak upward trend (0.02 days/year) of the EPDs-SC during 1979–2013, the seasonal mean temperature averaged over SC also shows a significant upward linear trend of 0.031 °C/year at the 99% confidence level. In contrast, during the same period, the EPDs-NC has almost no trend (0.004 days/year) despite the significant (at 99% confidence level) upward trend of 0.032 °C/year in seasonal mean temperature averaged over NC. This may suggest a region-independent extreme precipitation changes in the context of global warming.

4 Physical interpretation of regional EPDs indices

What physical processes govern the variability of EPDs over SC and NC? To address this question, we first examine the large-scale lower boundary anomalies concurring with the EPDs-SC and EPDs-NC.

Associated with increased EPDs-SC is the enhanced MJ rainfall anomaly over South China (Fig. 5a). To its south is a vast zone of suppressed rainfall band stretching from the western to eastern North Pacific (Fig. 5a). A pronounced anticyclone anomaly appears over the Philippine Sea (Fig. 5b), resulting in enhanced moist southwesterlies along the northwest flank of the anticyclone and increased EPDs over South China. Note that the anomalous anticyclone around the Philippine Sea coexists with warmer (colder) SST to the west (east) of its center (Fig. 5c). Besides, it is seen that strong positive SST anomalies over the eastern equatorial Pacific and tropical Indian Ocean are associated with increased EPDs-SC (Fig. 5c).

The evolution of the equatorial Indo-Pacific SST anomalies that associated with the EPDs-SC (Fig. 6a) suggests that EPDs-SC is increased during the rapid decaying phase of central-eastern Pacific El Nino. The way whereby El Nino has prolonged influence on Asian summer monsoon

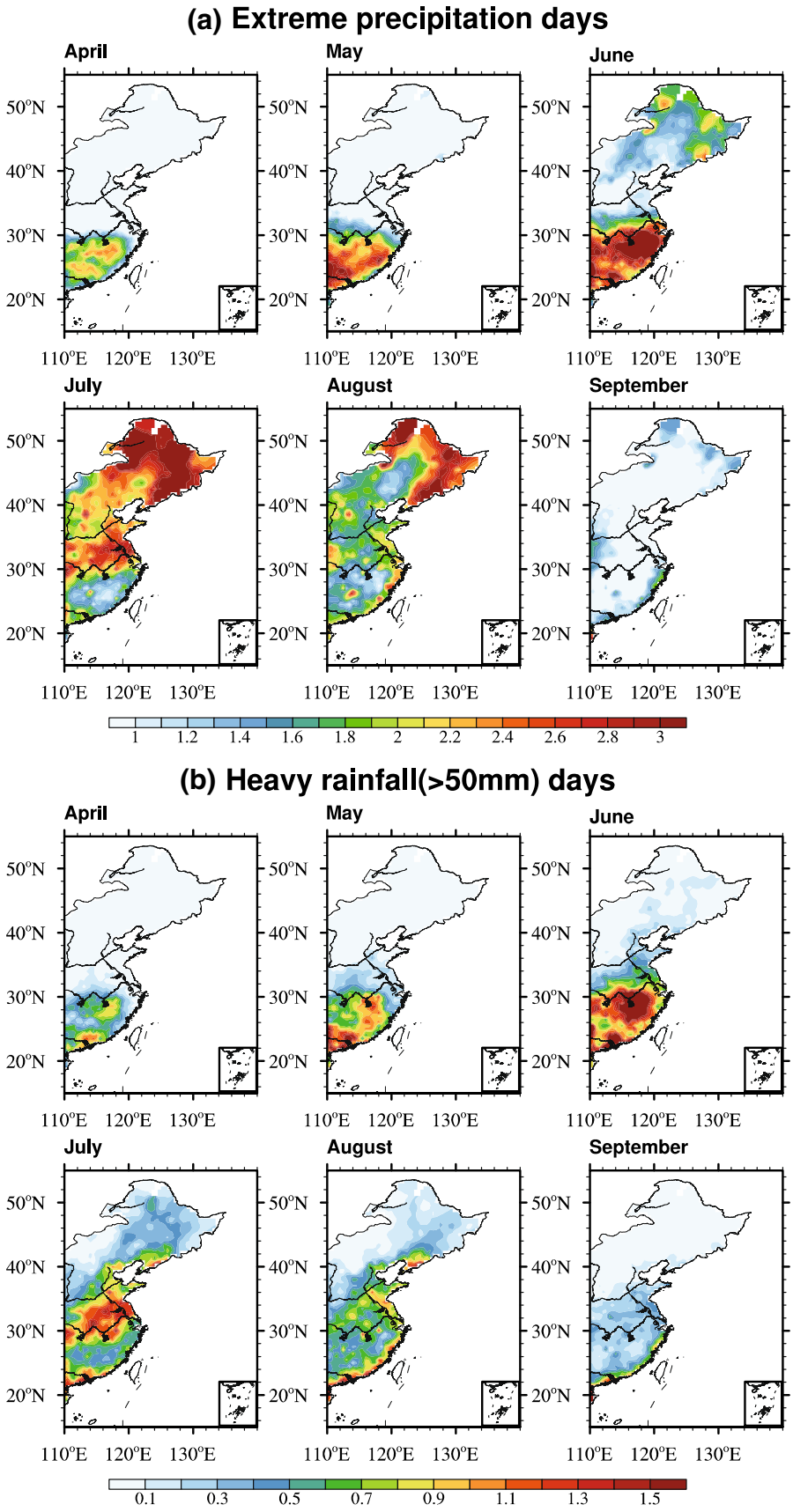

Fig. 2 The climatological monthly mean **a** EPDs in April, May, June, July, August, and September over eastern China. **b** The same as **a** except for heavy rainfall (daily rainfall > 50 mm) days

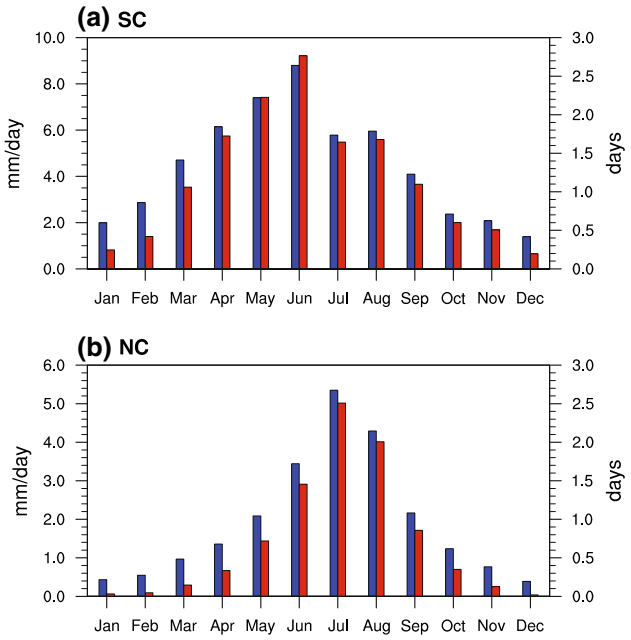

Fig. 3 Climatological annual cycle of monthly mean precipitation (*blue bar, left axis*) and monthly EPDs (*red bar, right axis*) averaged over **a** South China and **b** northern China

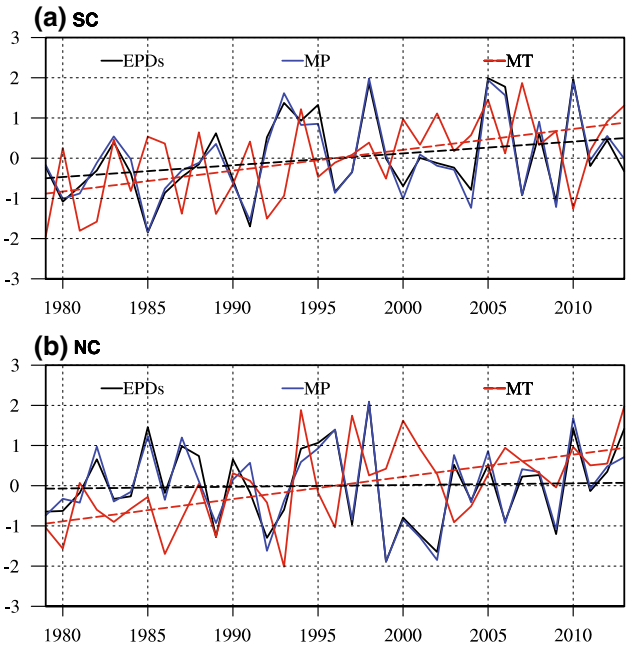

Fig. 4 Time series of EPDs, mean precipitation (MP) and mean temperature (MT) averaged over **a** SC in May–June. **b** The same as **a** except for NC in July–August. All time series are normalized by their own standard deviations. *Black* (*red*) *dashed lines* indicate the linear trend of EPDs (MT)

is through a persistent western North Pacific (WNP) anticyclonic anomaly (Wang et al. 2000, 2003). The anticyclone around WNP attains the maximum intensity after El Nino matures, and persists to the subsequent summer through a positive air–sea feedback between the WNP anticyclone and the SST dipole with cold water to the east and warm water to the west of the anticyclone center (Wang et al. 2000, 2003). An alternative explanation is that the Indian Ocean warming may induce a Kelvin wave easterly that generates anticyclonic vorticity over the Philippine Sea (Xie et al. 2009; Wu et al. 2010). However, Fig. 5b shows that the Indian Ocean warming does not generate significant Kelvin wave easterly anomaly because the warming does not cause sufficiently strong precipitation anomaly. It is the precipitation anomaly that can excite atmospheric Kelvin waves, not the warm SST itself.

During JA, associated with the increased EPDs-NC is the enhanced precipitation centered on northern China (Fig. 5d). An anticyclonic anomaly is found to the south of Japan (Fig. 5e) where the climatological ridge of the western North Pacific subtropical high (WNPSH) locates, implying that an enhanced WNPSH is linked to the increased EPDs over northern China. The associated strong southwesterly anomalies along the west flank of the anticyclonic anomaly (Fig. 5e) transport moisture farther to the north, favoring the convergence over northern China. Meanwhile, an anomalous cyclonic circulation over northern China (Fig. 5e) can also strengthen the local convergence, leading to an increase of EPDs over northern China. Thus, the enhanced zonal SLP contrast between the WNPSH and East Asian continent low plays a prominent role in affecting EPDs over northern China. Moreover, weak SST cooling can be seen in the eastern equatorial Pacific (Fig. 5f). To scrutinize the equatorial SST variation associated with EPDs-NC, we may examine Fig. 6b. The results in Fig. 6b indicate that EPDs-NC tend to increase when the eastern Pacific changes from a moderate warming in the previous winter to a weak cooling in the concurrent summer. Because of the weak cooling, change in the Pacific Walker cell is not evident (Fig. 5e). Although the cooling is weak, it still suppresses precipitation along the intertropical convergence zone and the monsoon trough in the southeast of the Philippines (Fig. 5d). The latter can directly strengthen the WNPSH through excitation of descending Rossby waves.

Note that the seasonal evolution of the WNPSH is the main factor modulating EPDs over eastern China. From MJ to JA, rainfall belt propagates northward from southern to northern China, which corresponds to the seasonal march of low level (850 hPa) anomalous WNP anticyclone from the Philippine Sea to the south of Japan. ENSO in the preceding winter and the local air–sea interaction over Indo-Pacific warm pool play key roles in affecting the EPDs over eastern China via modifying the location and strength of the WNPSH.

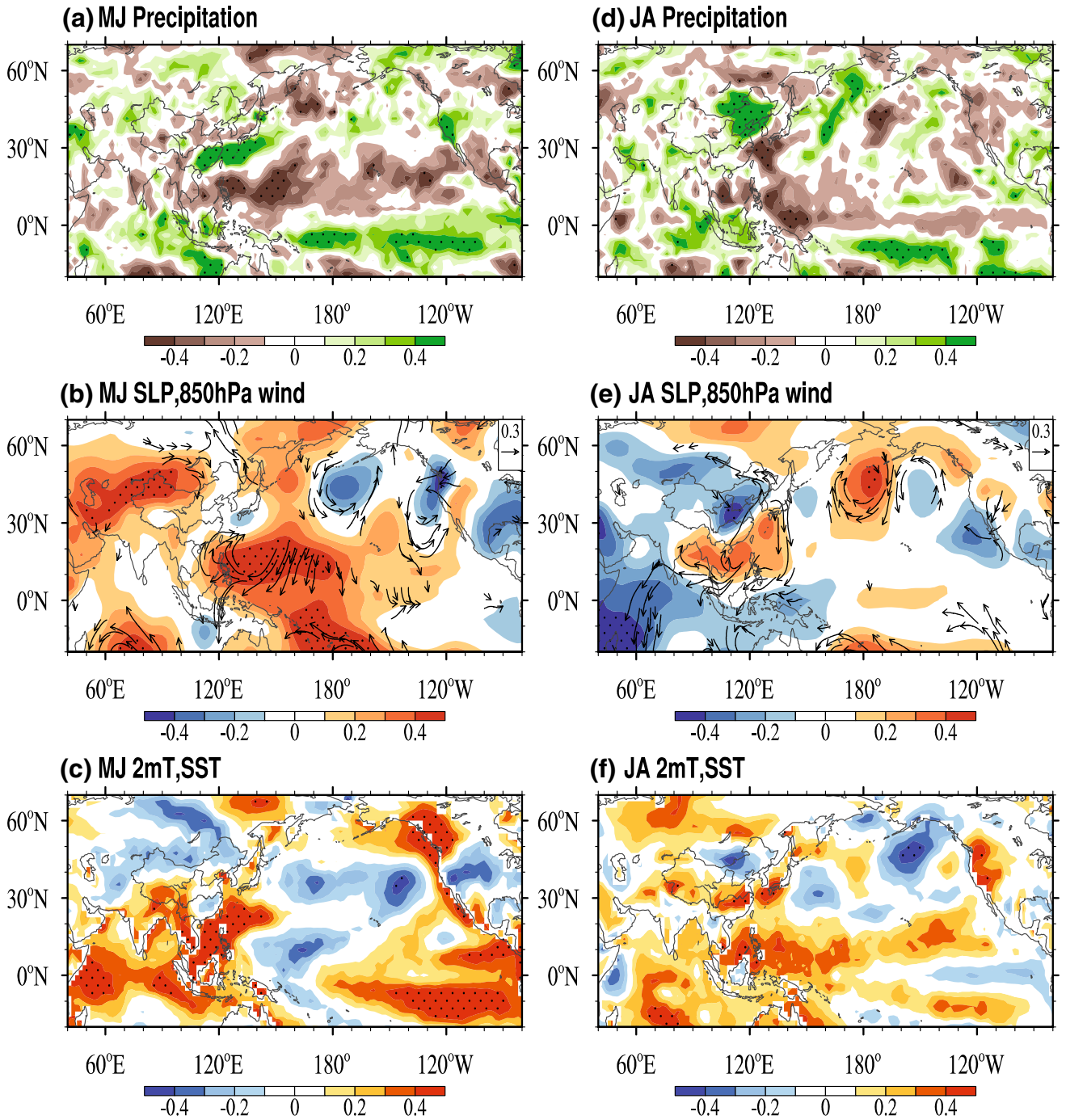

Fig. 5 Simultaneous correlation fields between EPDs-SC and **a** precipitation (*shading*), **b** SLP (*shading*), 850 hPa wind (*vectors*), **c** SST (*shading*) in May–June (MJ) during 1979–2000. **d–f** The same as **a–c**, respectively, but for EPDs-NC in July–August (JA). *Dotted areas* denote regions with correlation coefficients significant at 95% confidence level

5 Physical predictors for each regional EPDs index

The simultaneous large-scale anomalies associated with each regional EPDs index provide dynamical insights for selecting physically meaningful predictors. For each EPDs index, one or two predictors (black box in Fig. 7) are selected for construction of P-E prediction model. These predictors are highly correlated (99% confidence level) with predictand and independent with each other (Table 1). Other physical predictors are excluded because of their dependencies on the selected predictors.

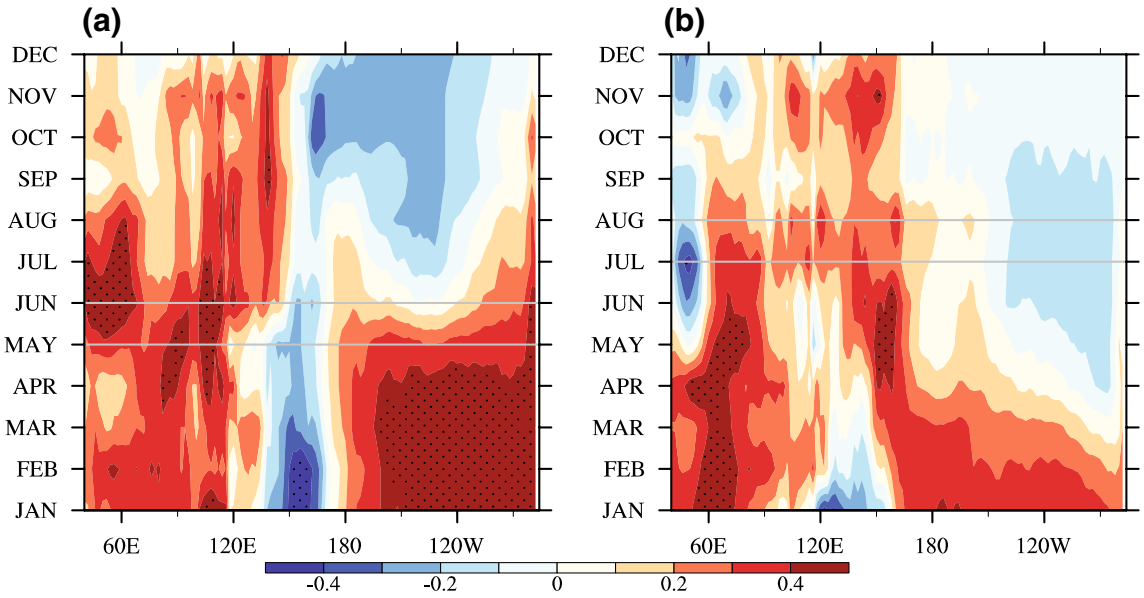

Fig. 6 The lead–lag correlation coefficients between equatorial Indo-Pacific (40°E–80°W) SST anomalies averaged between 5°S and 5°N and **a** EPDs-SC, **b** EPDs-NC during 1979–2000. The *dots* represent the correlation coefficient significant at the 95% confidence level

For EPDs-SC, one predictor SC-a is selected, which features high SLP anomalies over the WNP during March–April (Fig. 7a). The high SLP anomalies maintain and enhance the WNPSH in the ensuing MJ (Fig. 8a) through the local air–sea interaction between the WNPSH and the cold (warm) SST to its east (west) (Fig. 8b). The associated southwesterlies along the northwest flank of the WNPSH transport warm moisture into South China, leading to intensified precipitation over SC (Fig. 8a, c).

Two tendency predictors are selected for EPDs-NC. The first predictor, NC-a, is a long-term dipole SST tendency with cooling in the tropical central-eastern Pacific and warming in the tropical western Pacific from Dec.–Jan. to May–June (Fig. 7b), which is corresponding to the developing phase of La Nina (Fig. 6b). This east–west dipole SST tendency can strengthen the equatorial easterlies through zonal thermal gradients, thus leading to a central-eastern Pacific cooling in the following JA (Fig. 9a). The central-eastern Pacific cooling generates westward propagating descending Rossby waves through suppressed convection over WNP. The Rossby wave response enhances the WNPSH and thus transports moisture farther to the north, increasing EPDs-NC (Fig. 9b-c). The second predictor NC-b denotes a 2-m warming tendency over central Eurasia from Dec.–Jan. to May–June (Fig. 7c). This warming tendency persists to the following JA and foreshadows a high anomaly in situ at 200 hPa (Fig. 10a), which leads to a downstream low SLP anomaly disturbance centered over central China in JA (Fig. 10b). This low SLP anomaly favors local convergence and moisture transporting, thus increasing precipitation over NC (Fig. 10b, c).

6 Predictability of EPDs over Eastern China

Based on the abovementioned physical predictors, a suite of stepwise regression prediction equations is established for each EPDs index. As shown in Fig. 11, the cross-validated reforecast and independent forecast EPDs indices made by the P–E models are capable of capturing the interannual variation of observed EPDs indices, suggesting that the P–E models have a good capacity to predict the EPDs over eastern China. For EPDs-SC, the TCC (MSSS) skill of cross-validated reforecast during 1979–2000 is 0.62 (0.37). When the P–E model is built using 1979–2000 data, the independent forecast has significant TCC skill (95% confidence level) of 0.60 for the recent 13 years (2001–2013). The forecast skills for EPDs-NC are higher. TCC skills from both cross-validated reforecast (0.83) and independent forecast (0.74) are significant at 99% confidence level. Note that the two predictors for EPDs-NC are independent (Table 1), therefore, they are highly complementary, which raises the hindcast skill (Wang et al. 2015b). The superior skills contributed by P–E models provide a benchmark for the lower bound of predictability of EPDs over eastern China for current forecast year.

7 Summary and discussion

The present study investigates the predictability sources and assesses the predictability of summer EPDs over eastern China. The major conclusions are summarized as follow:

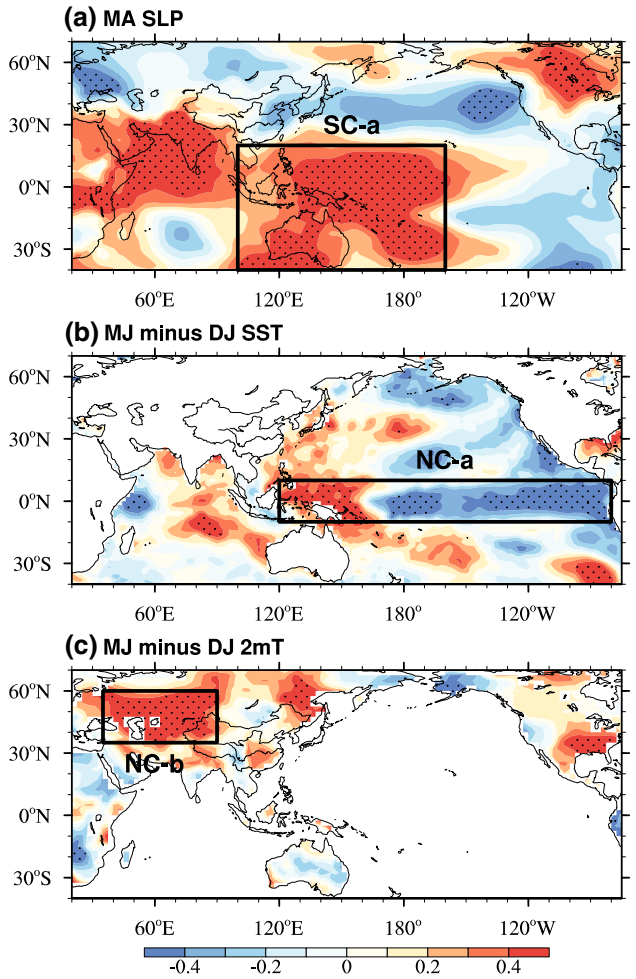

Fig. 7 The correlation maps between **a** EPDs-SC and March–April mean SLP, **b** EPDs-NC and May–June minus Dec.–Jan. SST, and **c** EPDs-NC and May–June minus Dec.–Jan. 2mT during 1979–2000. The *box regions* show the locations of predictor SC-a (40°S–20°N, 100°E–160°W), NC-a (10°S–10°N, 120°E–80°W), and NC-b (35°N–60°N, 35°E–90°E) in **a**–**c**, respectively. *Dotted areas* denote regions with correlation coefficients significant at 95% confidence level

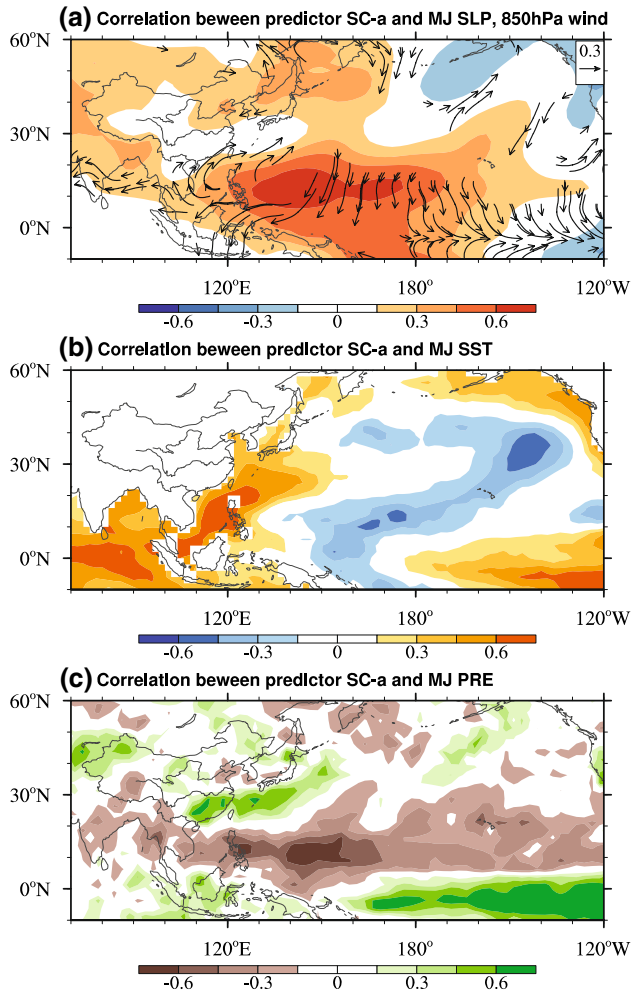

Fig. 8 The lead-lag correlation maps between predictor SC-a and May–June mean **a** SLP (*shading*), 850 hPa wind (*vector*), **b** SST (*shading*) and **c** precipitation (*shading*) during 1979–2000

Table 1 The correlation coefficients between EPDs-SC/EPDs-NC and corresponding predictors (SC-x/NC-x) and among each other (1979–2000)

	EPDs-SC	
SC-a	**0.71**	
	EPDs-NC	NC-a
NC-a	**0.56**	
NC-b	**0.78**	0.27

The bold numbers denote statistically significant at 99% confidence level

1. The EPDs over SC have peaks in MJ, while EPDs over NC have peaks in JA. Two summer regional EPDs indices (EPDs-SC, EPDs-NC) can therefore be defined by areal-mean EPDs in their own EPDs peak seasons, thus facilitating the study of the large-scale hydrological hazards.
2. During MJ, the EPDs-SC is increased in the rapid decaying phase of El Nino. Associated with the increased EPDs-SC is a pronounced anticyclone anomaly around the Philippine Sea, which is maintained through interaction between the WNP anomalous high and underlying dipolar SST anomalies in the northern Indo-Pacific warm pool. The enhanced Philippine Sea anticyclone leads to enhance northward moisture transportation to SC.
3. During JA, associated with the increased EPDs-NC is a zonal SLP dipole with WNP anomalous high and East Asian continent low. This situation occurs during a transition from a moderate warming in the preceding winter to a weak cooling in the eastern Pacific. The WNP anomalous high is partially enhanced by the eastern Pacific cooling-induced suppressed convection in

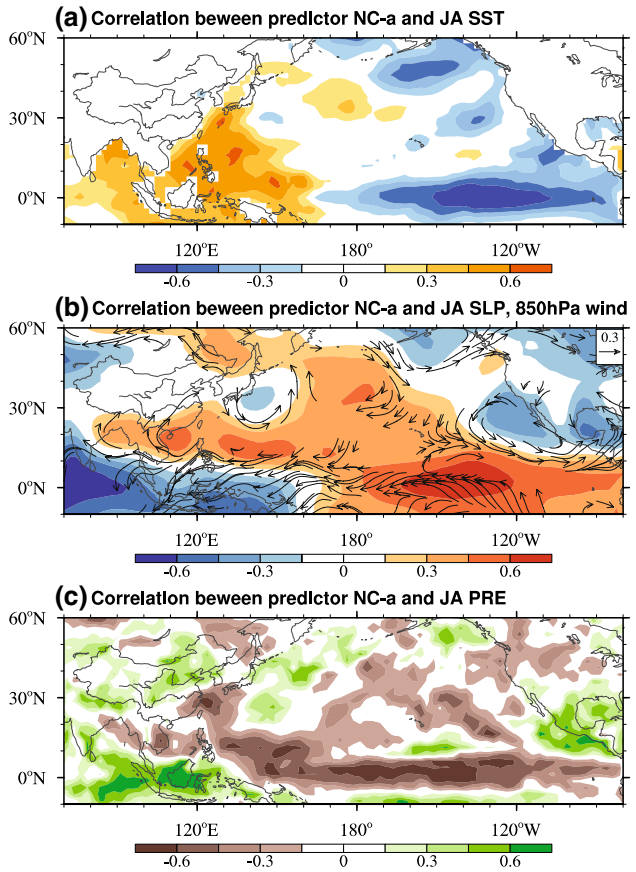

Fig. 9 The lead-lag correlation maps between predictor NC-a and July–August mean **a** SST (*shading*), **b** SLP (*shading*), 850 hPa wind (*vector*) and **c** precipitation (*shading*) during 1979–2000

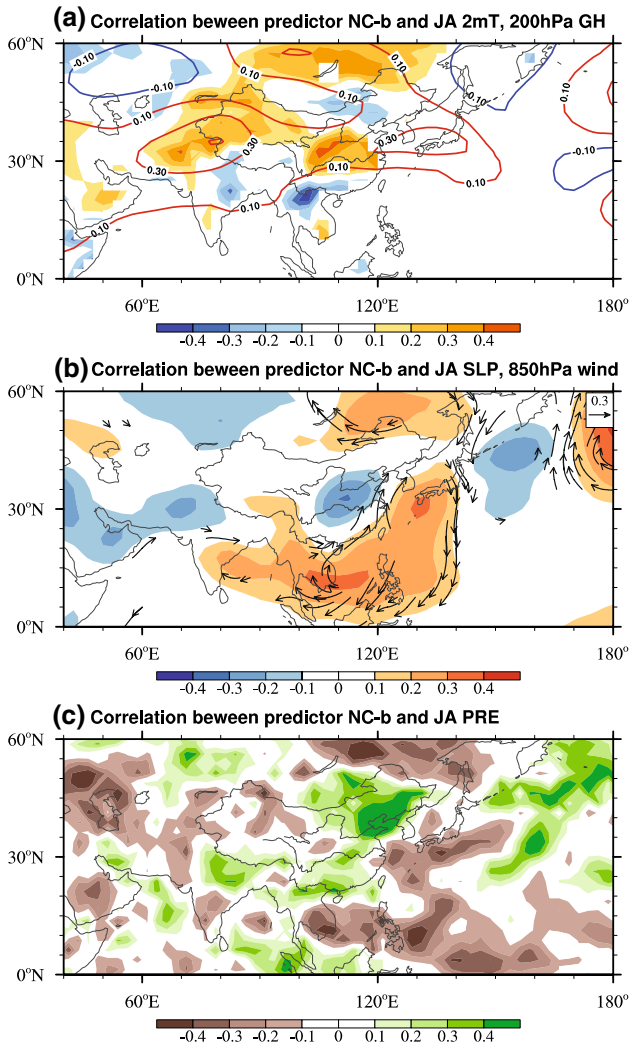

Fig. 10 The lead-lag correlation maps between predictor NC-b and July–August mean **a** 2-m temperature (*shading*), 200 hPa geopotential height (*contour*), **b** SLP (*shading*), 850 hPa wind (*vector*) and **c** precipitation (*shading*) during 1979–2000

the western Pacific monsoon trough via emanation of descending Rossby waves. The strengthened southerly anomalies between the anomalous WNPSH and East Asian low transport moisture to northern China and enhance precipitation over NC.

4. The increased EPDs-SC is preceded by a high SLP anomaly over the western Pacific, which signifies atmosphere–ocean interaction between the high and dipolar SST anomalies. We also found two precursors for EPDs-NC: a zonal dipole SST tendency over the equatorial Pacific and a 2-m temperature tendency over central Eurasia. The possible causative linkages between these predictors and corresponding predictands were discussed.
5. To access the predictability of EPDs-SC and EPDs-NC, a set of P-E prediction models was built using above-mentioned physical predictors. The cross-validated reforecast (independent forecast) of EPDs for 1979–2000 (2001–2013) achieves significant TCC skill of 0.62, 0.83 (0.60, 0.74) for SC and NC, respectively. These superior skills derived from P–E models offer an estimation of the lower bound of predictability for summer EPDs over eastern China for current forecast year. Compared to the potential predictability of extreme precipitation in China estimated by statistical method (Wei et al. 2017), the present study provides higher predictability with clearer physical meaning.

We found that the summer EPDs are highly correlated with the summer mean rainfall. Thus, variations of the seasonal mean rainfall and EPDs share similar origins and predictability sources. In other words, the prediction skill for summer EPDs largely arises from the prediction skill of the summer mean rainfall.

Since the mean states in MJ and JA are quite different (Wang et al. 2009b), prediction using separate bi-monthly

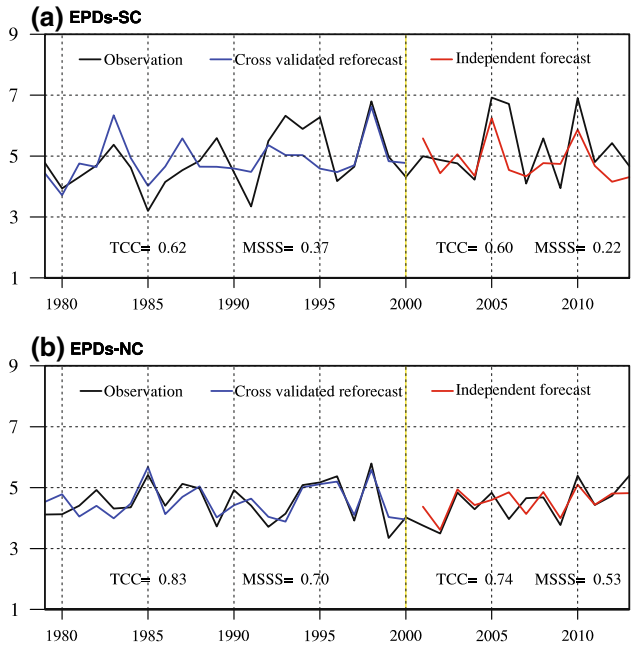

Fig. 11 Time series of **a** EPDs-SC and **b** EPDs-NC obtained from observation (*black line*), cross-validated reforecast (*blue line*) and independent forecast (*red line*)

(MJ and JA) anomalies rather than common JJA anomalies can considerably improve the prediction skills.

Although prediction skills of EPDs derived from P–E models are superior, there are caveats and limitations. First, the predictand-predictors relationship derived from the current 22 years (1979–2000) may experience secular changes or abrupt changes, which may cause low forecast skills. The prediction models presented in this study may not fully applicable for other periods. Because East Asian summer monsoon underwent a substantial decadal change in the late 1970s (Hu 1997; Ding et al. 2008; Zhou et al. 2009), the corresponding causative physical mechanism could be different before and after the late 1970s (Wu and Wang 2002; Ding et al. 2009). Thus, the physical predictors selected during period of 1979–2000 are not significantly correlated with predictands before 1979: the correlation coefficient is 0.27 between EPDs-SC and SC-a, 0.29 between EPDs-NC and NC-a, 0.20 between EPDs-NC and NC-b for 1960–1978, resulting in lower forecast skill when prediction models are built using data of 1960–2000. The nonstationarity of the predictor–predictand relationships has been a common major challenge and limitation for empirical prediction methods. Prediction of pre-1979 extreme events really requires a separate set of prediction equation. It calls for future study concerning why the relationships have been changed and how to anticipate another future change of the relationships. Second, since all the data from the period of 1979–2000 is used to select the predictors, the 22-year (1979–2000) cross-validated reforecast skills are likely to be inflated (DelSole and Shukla 2009). Third, the causative processes linking the predictors and predictands proposed in the present study are considered as a speculation, further validations via well-designed numerical experiments are needed.

Acknowledgements This study is supported by the Atmosphere–Ocean Research Center (AORC) and International Pacific Research Center (IPRC) at University of Hawaii and the National Research Foundation (NRF) of Korea through a Global Research Laboratory (GRL) Grant of the Korean Ministry of Education, Science and Technology (MEST, #2011–0021927). The AORC is partially funded by Nanjing University of Information Science and Technology (NUIST). This is the NUIST-Earth System Modeling Center (ESMC) publication number 174, the School of Ocean and Earth Science and Technology publication number 1280, the IPRC publication number 10112. The authors declare that they have no conflict of interest.

References

Adler RF et al (2003) The version-2 global precipitation climatology project (GPCP) monthly precipitation analysis (1979–Present). J Hydrometeorology 4:1147–1167

Alexander LV et al (2006) Global observed changes in daily climate extremes of temperature and precipitation. J Geophys Res Atmos 111:D05109

Blockeel H, Struyf J (2003) Efficient algorithms for decision tree cross-validation. J Mach Learn Res 3:621–650

Choi G et al (2009) Changes in means and extreme events of temperature and precipitation in the Asia-Pacific Network region, 1955–2007. Int J Climatol 29:1906–1925

Dee DP et al (2011) The ERA-Interim reanalysis: configuration and performance of the data assimilation system. Q J R Meteorol Soc 137:553–597

DelSole T, Shukla J (2009) Artificial skill due to predictor screening. J Clim 22:331–345

Ding Y, Wang Z, Sun Y (2008) Inter-decadal variation of the summer precipitation in East China and its association with decreasing Asian summer monsoon. Part I: Observed evidences. Int J Climatol 28:1139–1161

Ding Y et al (2009) Inter-decadal variation of the summer precipitation in China and its association with decreasing Asian summer monsoon Part II: possible causes. Int J Climatol 29:1926–1944

Donat MG et al (2016) More extreme precipitation in the world's dry and wet regions. Nat Clim Change 6:508–513

Easterling DR et al (2000) Observed variability and trends in extreme climate events: a brief review. Bull Am Meteorol Soc 81:417–426

Gao X, Zhao Z, Filippo G (2002) Changes of extreme events in regional climate simulations over East Asia. Adv Atmos Sci 19:927–942

Geisser S (1975) The predictive sample reuse method with applications. J Am Stat Assoc 70:320–328

Grunseich G, Wang B (2016) Predictability of arctic annual minimum sea ice patterns. J Clim 29:7065–7088

Hu Z-Z (1997) Interdecadal variability of summer climate over East Asia and its association with 500 hPa height and global sea surface temperature. J Geophys Res Atmos 102:19403–19412

Huang B et al (2015) Further exploring and quantifying uncertainties for extended reconstructed sea surface temperature (ERSST) version 4 (v4). J Clim 29:3119–3142

Lee J-Y et al (2013) Seasonal prediction and predictability of the Asian winter temperature variability. Clim Dyn 41:573–587

Lesk C, Rowhani P, Ramankutty N (2016) Influence of extreme weather disasters on global crop production. Nature 529:84–87

Li J, Wang B (2016) How predictable is the anomaly pattern of the Indian summer rainfall? Clim Dyn 46:2847–2861

Li J, Dong W, Yan Z (2012) Changes of climate extremes of temperature and precipitation in summer in eastern China associated with changes in atmospheric circulation in East Asia during 1960–2008. Chin Sci Bull 57:1856–1861

Li Z et al (2016) Comparison of two homogenized datasets of daily maximum/mean/minimum temperature in China during 1960–2013. J Meteorol Res 30:53–66

Li J, Zhu Z, Dong W (2017a) A new mean-extreme vector for the trends of temperature and precipitation over China during 1960–2013. Meteorol Atmos Phys 129:273–282

Li J, Wang B, Yang Y-M (2017b) Retrospective seasonal prediction of summer monsoon rainfall over West Central and Peninsular India in the past 142 years. Clim Dyn 48:2581–2596

Liu R et al (2015) Trends of extreme precipitation in eastern China and their possible causes. Adv Atmos Sci 32:1027–1037

Meehl GA et al (2000) An introduction to trends in extreme weather and climate events:Observations,socioeconomic impacts,terrestrial ecological impacts,and model projections. B Am Meteorol Soc 81:413–416

Meehl GA et al (2007) Global climate projection. Climate change 2007: the physical science basis. Contribution of working group I to the fourth assessment report of the Intergovernmental Panel on Climate Change. Cambridge University Press, Cambridge

Moberg A et al (2006) Indices for daily temperature and precipitation extremes in Europe analyzed for the period 1901–2000. J Geophys Res Atmos 111:D22106

Murphy AH (1988) Skill scores based on the mean square error and their relationships to the correlation coefficient. Mon Weather Rev 116:2417–2424

Orsolini YJ et al (2015) Extreme precipitation events over north China in August 2010 and their link to eastward-propagating wave-trains across Eurasia: observations and monthly forecasting. Q J R Meteorol Soc 141:3097–3105

Rayner NA et al (2003) Global analyses of sea surface temperature, sea ice, and night marine air temperature since the late nineteenth century. J Geophys Res 108:4407

Tu K, Yan Z, Dong W (2010) Climatic jumps in precipitation and extremes in drying North China during 1954–2006. J Meteorol Soc Jpn Ser II 88:29–42

Wang B, LinHo (2002) Rainy season of the Asian–Pacific summer monsoon. J Clim 15:386–398

Wang F, Yang S (2017) Regional characteristics of long-term changes in total and extreme precipitations over China and their links to atmospheric–oceanic features. Int J Climatol 37:751–769

Wang B, Wu R, Fu X (2000) Pacific-east Asian teleconnection: how does ENSO affect east Asian climate? J Clim 13:1517–1536

Wang B, Wu R, Li T (2003) Atmosphere–warm ocean interaction and its impacts on Asian–Australian Monsoon variation. J Clim 16:1195–1211

Wang B et al (2009a) Advance and prospectus of seasonal prediction: assessment of the APCC/CliPAS 14-model ensemble retrospective seasonal prediction (1980–2004). Clim Dyn 33:93–117

Wang B et al (2009b) Distinct principal modes of early and late summer rainfall anomalies in East Asia. J Clim 22:3864–3875

Wang B, Lee J-Y, Xiang B (2015a) Asian summer monsoon rainfall predictability: a predictable mode analysis. Clim Dyn 44:61–74

Wang B et al (2015b) Rethinking Indian monsoon rainfall prediction in the context of recent global warming. Nat Commun 6:7154

Wei W, Yan Z, Jones PD (2017) Potential predictability of seasonal extreme precipitation accumulation in China. J Hydrometeorol 18:1071–1080

Weng H et al (2004) Interannual-interdecadal variation in large-scale atmospheric circulation and extremely wet and dry summers in China/Japan during 1951–2000 Part I: spatial patterns. J Meteorol Soc Jpn Ser II 82:775–788

WMO (2002) Standardised verification system for longrange forecasts (LRF): new attachment II-9 to the manual on the GDPS, WMO No. 485. WMO, Geneva

Wu R, Wang B (2002) A contrast of the east Asian Summer Monsoon–ENSO relationship between 1962–77 and 1978–93. J Clim 15:3266–3279

Wu B, Li T, Zhou T (2010) Relative contributions of the Indian Ocean and local SST anomalies to the maintenance of the Western North Pacific anomalous anticyclone during the El Niño decaying summer. J Clim 23:2974–2986

Xie S-P et al (2009) Indian Ocean capacitor effect on Indo–Western Pacific climate during the summer following El Niño. J Clim 22:730–747

Xing W, Wang B, Yim S-Y (2016) Peak-summer East Asian rainfall predictability and prediction part I: Southeast Asia. Clim Dyn 47:1–13

Yim S-Y, Wang B, Xing W (2014) Prediction of early summer rainfall over South China by a physical-empirical model. Clim Dyn 43:1883–1891

You Q et al (2010) Changes in daily climate extremes in China and their connection to the large scale atmospheric circulation during 1961–2003. Clim Dyn 36:2399–2417

Zhai P et al (2005) Trends in total precipitation and frequency of daily precipitation extremes over China. J Clim 18:1096–1108

Zhang D, Feng G, Hu J (2008) Trend of extreme precipitation events over China in last 40 years. Chin Phys B 17:736

Zhou T et al (2009) Detecting and understanding the multi-decadal variability of the East Asian Summer Monsoon Recent progress and state of affairs. Meteorol Z 18:455–467

Zhou T et al (2013) The 2012 North China floods: explaining an extreme rainfall event in the context of a longer-term drying tendency. B Am Meteorol Soc 94:S49–S51

Zhu Z, Li T (2017) Empirical prediction of the onset dates of South China Sea summer monsoon. Clim Dyn 48:1633–1645